Dyes and Pigments 129 (2016) 34–42

Contents lists available at ScienceDirect

Dyes and Pigments

journal homepage: www.elsevier.com/locate/dyepig

A bipolar emitting material for high efficient non-doped fluorescent organic light-emitting diode approaching standard deep blue

Shigen Fan [a, b], Jing You [a, b, *], Yanqin Miao [c], Hua Wang [c], Qingyun Bai [c], Xicheng Liu [a, b], Xianggao Li [a, b], Shirong Wang [a, b, **]

[a] Tianjin University, School of Chemical Engineering and Technology, Tianjin 300072, China
[b] Collaborative Innovation Center of Chemical Science and Engineering, Tianjin 300072, China
[c] Key Laboratory of Interface Science and Engineering in Advanced Materials, Taiyuan University of Technology, Ministry of Education, No. 79 Yingze Street, Taiyuan 030024, Shanxi, China

ARTICLE INFO

Article history:
Received 13 November 2015
Received in revised form
2 February 2016
Accepted 6 February 2016
Available online 12 February 2016

Keywords:
Twisted structure
Thermal stability
Bipolar characteristic
Non-doped
Fluorescent
Deep blue

ABSTRACT

A deep blue emitting compound 9-(4′-(1,4,5-triphenyl-1*H*-imidazol-2-yl)-[1,1′-biphenyl] -4-yl)-9*H*-carbazole was designed and synthesized. The emitting compound characters as donor-π-acceptor structure with carbazole as the electron-donor and imidazole as the electron-acceptor. The emitting compound shows high quantum yield (0.87) in solution and good thermal stability. The emitting compound exhibits bipolar transporting characteristics identified by single-carrier devices. The non-doped fluorescent organic light-emitting diode with the emitting compound as emitting layer exhibits emission peak at 420 nm and full width at half maximum of 54 nm, maximum current efficiency of 2.30 cd/A, and maximum power efficiency of 1.52 lm/W, which are higher than most reported deep blue emitters with a ***y*** coordinate ≤0.064. The chromaticity coordinate is stable at (0.166, 0.064) with increasing operation voltage.

1. Introduction

Organic light-emitting diode (OLED) has been the research hotspot in both academic and industrial fields, since first reported by C.W. Tang's group [1–4]. The deep blue OLED is one of the key technique for realization of both full-color display and solid-state lighting [5–8]. The intrinsic nature of wide energy gap (≥3 eV) of deep blue emitting materials results in low electron affinity which has negative effect on the charge injection and charge balance in devices [9,10], Therefore, the performance of deep blue OLEDs is much lower than green and red devices [7], which limits the development of OLEDs industry.

Balancing the charge transport is one of the most important factors to obtain high efficient OLEDs [11–13]. Very recently, bipolar materials characterized with electron-donor and electron-acceptor are becoming a new strategy to improve the balance of charge injection and transport in OLEDs [11,12,14]. This kind of emitting materials can improve the device performance by balancing both holes and electrons transporting in the emitting layer, facilitating exciton formation and broadening the exciton formation zone [15–18]. However, intramolecular charge-transfer (ICT) of donor and acceptor moieties leads to fluorescence bathochromic-shift [14,18]. Therefore, the bipolar deep blue materials always do not match the standard of European Broadcasting Union (EBU) with the Commission International de L'Eclairage (CIE) coordinates of (0.15, 0.06). J.H. Huang's group reported a series of bipolar emitting anthracene derivatives containing triphenylamine as electron-donor and benzimidazole moiety as electron-acceptor. The non-doped OLEDs exhibited CIE with ***y*** value in range of 0.12–0.23 [18]. A twisted donor-acceptor (D-A) triphenylamine-imidazol deep blue emitter TPA-PPI reported by W.J. Li et al., with which the ***y*** value of OLED approached to 0.11 due to the twisted molecular structure [19]. In the study of Z. Gao et al., triphenylamine was replaced by the lower electron-donating ability carbazole moiety, achieving ***y*** value 0.077 closing to the standard of EBU ($y = 0.06$) [20].

In this work, the bipolar molecule 9-(4′-(1,4,5-triphenyl-1*H*-imidazol-2-yl)-[1,1′- biphenyl]-4-yl)-9*H*-carbazole (CzB-PIM) with carbazole moiety as the mild electron-donor and bukyl N1,C4,C5-

* Corresponding author. Tianjin University, School of Chemical Engineering and Technology, Tianjin 300072, China. Tel.: +86 22 27404208.
** Corresponding author. Tianjin University, School of Chemical Engineering and Technology, Tianjin 300072, China. Tel.: +86 22 27404208.
E-mail addresses: Youj1983@tju.edu.cn (J. You), wangshirong@tju.edu.cn (S. Wang).

http://dx.doi.org/10.1016/j.dyepig.2016.02.006
0143-7208/

triphenyl imidazole as the electron-acceptor was designed and synthesized by incorporating the biphenyl group. The twisted structure can reduce the π-conjugation, increase band gap, and control the bathochromic-shift resulting from ICT [12,21], which could help to obtain deep blue emission. The molecular structure and synthetic route are showed in Scheme 1. The quantum yield of CzB-PIM was determined to be 0.87 with reference method in Tetrahydrofuran (THF) solution. The thermal stability of CzB-PIM was investigated with thermal gravity analysis (TGA) and differential scanning calorimetry (DSC). The CzB-PIM showed a good thermal stability with glass transition temperature (T_g) of 134 °C and decomposition temperature (T_d) of 413 °C. The good bipolar characteristics of CzB-PIM were proved by single-carrier devices. The non-doped Fluorescent OLED with CzB-PIM as emitting layer exhibited the maximal emission wavelength at 420 nm and full width at half maximum (FWHM) of 54 nm. The highest current efficiency was 2.30 cd/A without optimization. The OLED showed chromaticity coordinate stable at CIE (0.166, 0.064) with increasing operation voltage.

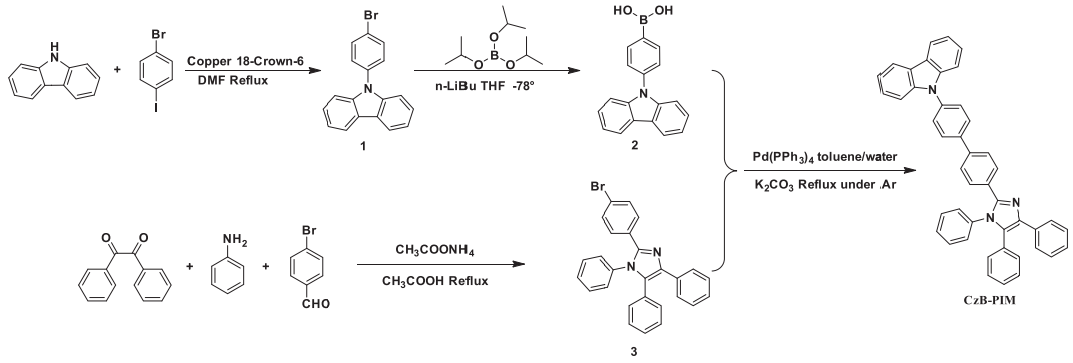

Scheme 1. Molecular structures and synthetic routes of CzB-PIM.

2. Experiment section

2.1. Materials

All materials were used as received from commercial supplier (Tianjin Heowns Biochemical Technology Co., Ltd.) without further purification. All solvents were purchased from Tianjin Guangfu Fine Chemical Research Institute. THF was freshly distilled from sodium/benzophenone under argon (Ar) atmosphere before use.

2.2. General procedures

^{1}H and ^{13}C NMR spectra were obtained on a Bruker ACF400 (400 MHz) spectrometer in chloroform-d ($CDCl_3$) or dimethyl sulfoxide-d_6 (DMSO-d_6) with tetramethylsilane as reference. High resolution mass spectra (HRMS) data were obtained on a Bruker MicrOTOF-Q II. Absorption spectra of THF solution and film were recorded on a Thermo Evolution 300 UV–Vis spectrophotometer. Photoluminescence spectra were recorded on a Hitachi F-4500 fluorescence spectrophotometer. Fluorescence quantum yield (Φ_f) of CzB-PIM (THF solution) was determined by reference method with quinine sulfate solution in 0.01 M H_2SO_4 (Φ_f = 0.54) as a reference [22]. DSC measurement was recorded on a TA Q20 instrument operated at a heating rate of 10 °C/min from 25 °C to 350 °C in a N_2. The T_g was determined from the second heating scan loop. TGA was recorded on a METTLER TOLEDO TGA/DSC1 Thermogravimetric Analyzer heating rate of 10 °C/min from 30 °C to 600 °C in a N_2. X-ray diffraction spectra were recorded on a Rigaku Miniflex 600 with 2θ range of 3°–20°, scanning at a rate of 1°/min. The photoelectron yield spectroscopy (PYS) was carried out on a Sumitomo PYS-202 ionization energy detection system to determine the highest occupied molecular orbital (HOMO) energy level of CzB-PIM [23]. The lowest unoccupied molecular orbital (LUMO) energy level was estimated by summing the HOMO energy with the optical band gap determined from the absorption onset edge. X-ray crystallography of CzB-PIM was collected at the temperature of 113 K on a Rigaku XtaLAB P200 diffractometer equipped with graphite-monochromated Mo Ka radiation (λ = 0.71073 Å). The structure was solved with the SHELXL-97 program, and the refinement was performed by a full-matrix least-squares technique based on F^2 with the SHELXL-97 program [24]. Crystallographic data reported in this paper had been deposited with the Cambridge Crystal Data Centre and CCDC No. 1403616. Quantum chemical calculation was performed on a Gaussian 03 program with the Beck's three-parameter exchange functional and the Lee-Yang-Parr's correlation functional (B3LYP) using 6-31G (d) basis sets [25]. The ground geometries were fully optimized and distributions of the HOMO and LUMO orbitals were achieved based on the optimized ground state.

2.3. OLED fabrication and measurements

The device was fabricated by thermal vacuum deposition on the pre-patterned indium tin oxide (ITO) glass substrate with sheet resistance of 15 Ω/sq. The ITO substrate was rinsed and sonicated consecutively with detergent water, deionized water, and acetone. Followed with drying in cabinet, then exposed to a UV-ozone environment for 10 min. After these processes, the substrate was transferred into a vacuum chamber for sequential deposition of all organic functional layers by thermal evaporation below a vacuum of 5 × 10^{-4} Pa. The deposition rates for organic materials, lithium fluoride (LiF), and aluminum (Al), were about 1.0, 0.1 and 3.0 Å/s, respectively. The thickness and deposition rates of the films are controlled by a quartz thickness monitor. The overlap between ITO anode and Al cathode is 3 mm × 3 mm, as the active emissive area of the devices.

The current-voltage-forward luminance characteristics of device were measured with a ST-900M luminance meter and a Keithley 2400 programmable voltage current source. CIE coordinates, EL spectra were obtained on the PR655 Spectra scan spectrometer. All samples were measured directly after fabrication in ambient atmosphere at room temperature in the darkroom without encapsulation.

2.4. Synthesis and characterizations

The intermediates 9-(4-bromophenyl)-9*H*-carbazole (compound 1), (4-(9*H*-carbazol-9-yl) phenyl) boronic acid (compound 2)

[26] and 2-(4-bromophenyl)-1,4,5-triphenyl-1*H*-imidazole (compound 3) [27] were prepared using a similar method previously reported. Then the final compound (CzB-PIM) was then successfully prepared in high yield by Suzuki cross-coupling reaction of the boronic derivative (compound 2) and bromide (compound 3). The target compound was fully characterized by NMR, HRMS, and single-crystal X-ray diffraction pattern.

2.4.1. 9-(4-bromophenyl)-9H-carbazole (compound 1)

A mixture of carbazole (8.00 g, 47.84 mmol), 1-bromo-4-iodobenzene (17.60 g, 62.20 mmol), copper powder (Cu, 9.12 g, 43.53 mmol), potassium carbonate (K_2CO_3, 26.45 g, 191.37 mmol), 18-Crown-6 (4.43 g, 16.75 mmol) and anhydrous *N*,*N*-Dimethylformamide (DMF, 200 mL) was added into flask. After stirring and degassing for 15 min, the reaction system was refluxed for 12 h in Ar. Then the mixture was cooling down to room temperature. After adding deionized water, the brown solid was achieved and purified by silica gel column chromatography with an eluent pure petroleum ether and then obtained white crystal, **compound 1**, 13.66 g (88.61%). Mp: 146–148 °C; ^{1}H NMR (400 MHz, $CDCl_3$): δ 8.12 (d, J = 7.7 Hz, 2H), 7.70 (d, J = 8.5 Hz, 2H), 7.39 (dt, J = 14.1, 8.1 Hz, 6H), 7.28 (t, J = 7.2 Hz, 2H). ^{13}C NMR (100 MHz, $CDCl_3$): δ 140.59, 136.78, 133.09, 128.69, 126.07, 123.47, 120.29, 109.52.

2.4.2. (4-(9H-carbazol-9-yl) phenyl) boronic acid (compound 2)

Compound 1 (4.83 g, 15.00 mmol) was put into the flask. THF (60 mL) was added with the syring. The air in the flask was replaced with Ar three times. Then the reaction solution was cooled down to −78 °C for 10 min. *N*-butyl lithium (11.25 mL, 1.6 mol/L in hexane solution) was dropped into above flask dropwise with the syring, then stirred for 1 h at −78 °C. Triisopropyl borate ($[(CH_3)_2CHO]_3B$, 5.20 mL, 22.50 mmol) was added into above solution and then stirred for 1 h at −78 °C. After that, the reaction solution was warmed slowly to room temperature and stirred overnight. Hydrochloric acid (HCl, 30 mL, 2 mol/L) was added into the flask and stirred for another 30 min. Dichloromethane was used to extract the product and the organic layer was dried over $MgSO_4$. After filtration, the solution was concentrated using rotary evaporator. Then the crude product was washed with pure petroleum ether to afford white powder, **compound 2**, 3.70 g (85.91%). ^{1}H NMR (400 MHz, DMSO-d_6): δ 8.25 (d, J = 7.2 Hz, 2H), 8.08 (dd, J = 23.0, 7.2 Hz, 2H), 7.61 (d, J = 7.4 Hz, 2H), 7.43 (s, 4H), 7.30 (s, 2H). ^{13}C NMR (100 MHz, DMSO-d_6): δ 140.43, 138.92, 136.39, 126.72, 125.84, 123.28, 120.97, 120.57, 110.17.

2.4.3. 2-(4-bromophenyl)-1,4,5-triphenyl-1H-imidazole (compound 3)

Benzil (4.20 g, 19.98 mmol), aniline (2.75 g, 29.53 mmol), 4-bromobenzaldehyde (3.76 g, 20.32 mmol), ammonium acetate (NH_4OAc, 15.00 g, 194.60 mmol), and acetic acid (HOAc, 80 mL) were added into flask, followed with refluxed for 12 h under Ar environment. The reaction solution was cooled down to room temperature, then deionized water was poured into flask, then filtered. The filtrate was purified by column chromatography with petroleum ether/ethyl acetate (20:1) as eluent. White powder, **compound 3**, was achieved 3.67 g (85.95%). Mp: 203–204 °C; ^{1}H NMR (400 MHz, $CDCl_3$): δ 7.62–7.55 (m, 2H), 7.37 (d, J = 8.6 Hz, 2H), 7.33–7.15 (m, 11H), 7.11 (dd, J = 7.8, 1.5 Hz, 2H), 7.03 (dd, J = 7.8, 1.4 Hz, 2H). ^{13}C NMR (100 MHz, $CDCl_3$): δ 145.75, 138.43, 136.89, 134.16, 131.47–131.00, 130.36, 129.28, 128.70–127.98, 127.39, 126.77, 122.71.

2.4.4. 9-(4′-(1,4,5-triphenyl-1H-imidazol-2-yl)-[1,1′-biphenyl]-4-yl)-9H-carbazole (CzB-PIM)

Compound 2 (2.07 g, 7.20 mmol), **compound 3** (2.71 g, 6.00 mmol), tetrakis(triphenyl phosphine)palladium ($Pd(PPh_3)_4$, 138.30 mg, 120.00 μmol), anhydrous K_2CO_3 (2.07 g, 15.00 mmol) and degassed mixture solution (methylbenzene: deionized water = 5:1) were added into flask, then reflux for 11 h under Ar. The reaction solution was cooled down to room temperature and extracted by dichloromethane. The organic phase was dried with anhydrous $MgSO_4$ and concentrated by rotary evaporator then purified by column chromatography with gradient petroleum and dichloromethane mixture. White powder, CzB-PIM, was achieved 2.61 g (70.87%). ^{1}H NMR (400 MHz, $CDCl_3$): δ 8.15 (d, J = 7.7 Hz, 2H), 7.78 (d, J = 8.4 Hz, 2H), 7.67–7.53 (m, 8H), 7.42 (dt, J = 8.1, 4.3 Hz, 4H), 7.34–7.19 (m, 11H), 7.13 (ddd, J = 17.2, 7.7, 1.9 Hz, 4H). ^{13}C NMR (100 MHz, $CDCl_3$): δ 146.47, 140.84, 139.75, 139.45, 137.14, 134.46, 131.17, 129.31, 128.68–127.77, 127.39, 126.74, 126.00, 123.46, 120.35, 120.03, 109.82. HRMS: calcd. for $C_{45}H_{31}N_3$ $[M + H]^+$ (m/z) 614.2591, found at 614.2611 ($[M + H]^+$).

3. Result and discussion

3.1. X-ray crystal structure

The colorless single crystal of CzB-PIM was achieved from evaporation of chlorobenzene solution. The molecular structure determined by single crystal diffraction is shown in Fig. 1a, corresponding data and structural parameters are summarized in supporting information Table S1.

As shown in Fig. 1a, the carbazole and imidazole form dihedral angle of ca. 90°, 45° with biphenyl center, respectively. The benzene moieties connected with N3, C33 and C26 in imidazole show a dihedral angle of ca. 64°, 17° and 77°, respectively. The twisted structure of CzB-PIM minishes the π-conjugation effectively, and suppresses the intermolecular charge transfer (ICT), In addition, the fluorescence quenching induced by aggregation in the solid state is also reduced [11,21].

The interaction of adjacent molecules is shown in Fig. 1b exiting C–H (benzene ring)···π (imidazole ring, 2.789 Å) and C–H (benzene ring)···π (benzene ring in C26 position, 2.796 Å and 2.820 Å) intermolecular interactions, which may lead to the bathochromic-shift both in photo- or electroluminance spectra in the films. While, the non-coplanar structure of CzB-PIM can weaken the close-packing in the film state and keep the molecule in a good amorphous state [28].

3.2. Thermal property and morphology

Thermal property of CzB-PIM was investigated by TGA and DSC. As shown in Fig 2a, T_d of CzB-PIM is 413 °C, which was defined as the temperature at 5% weight loss. The high T_d can prevent decomposition during both the vacuum deposition process and device operation [29]. The melting point (T_m), T_g and crystallization temperatures (T_c) of CzB-PIM are 293 °C, 134 °C and 185 °C, respectively, which are observed from DSC curves shown in Fig. 2b. The high T_g of CzB-PIM means good stability of the amorphous film during fabrication and operation of OLEDs [30,31].

X-ray diffraction (XRD) spectra were employed to investigate the crystallization properties and stability of the vacuum deposition films. As shown in Fig. 3, the film of CzB-PIM both before and after 24 h, 90 °C annealing exhibits same featureless spectra as compared to ITO substrate. This demonstrates the stable amorphous structure of CzB-PIM films fabricated with vacuum deposition.

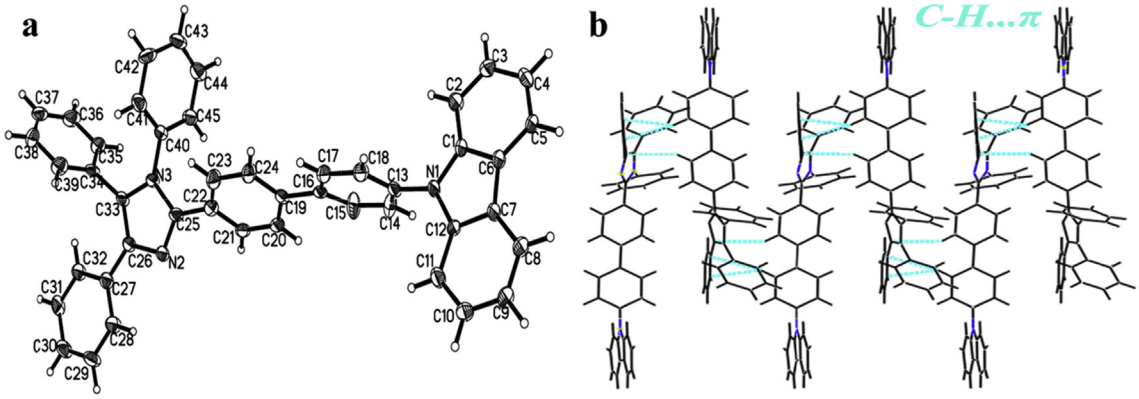

Fig. 1. Molecular structure (a); intermolecular interaction (b) for CzB-PIM (solvent chlorobenzene molecule are omitted for clarity).

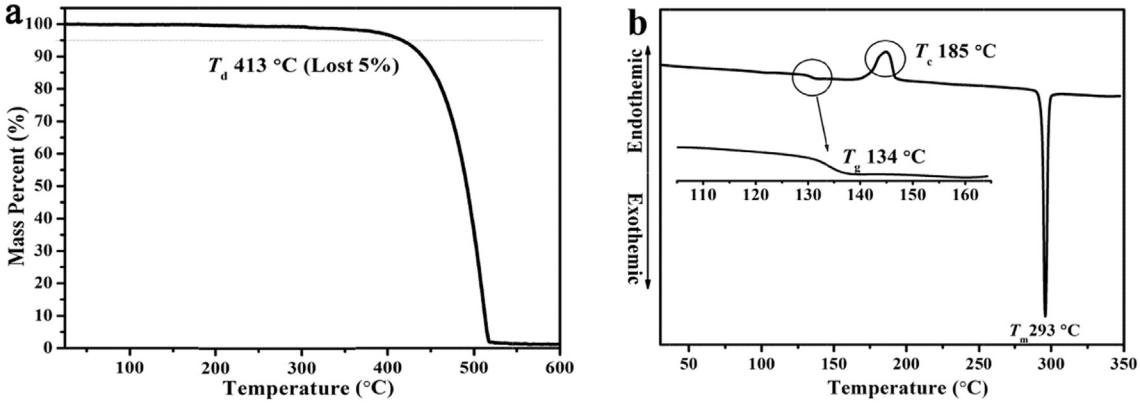

Fig. 2. TGA (a) and DSC (b) thermograms of CzB-PIM.

3.3. Optical properties

Normalized UV–Vis absorption and PL spectra of CzB-PIM in 10^{-5} M THF solution and thin film are shown in Fig. 4, corresponding data are summarized in Table 1. The absorption peaks in the range of 330–350 nm can be assigned to the π–π* transition of the substituent of 2-imidazole to the imidazole unit [20]. The absorption peak at 294 nm can be assigned the n-π* of carbazole [32,33]. The PL spectra with peak at 409 nm can be observed for CzB-PIM THF solution excited by 330 nm.

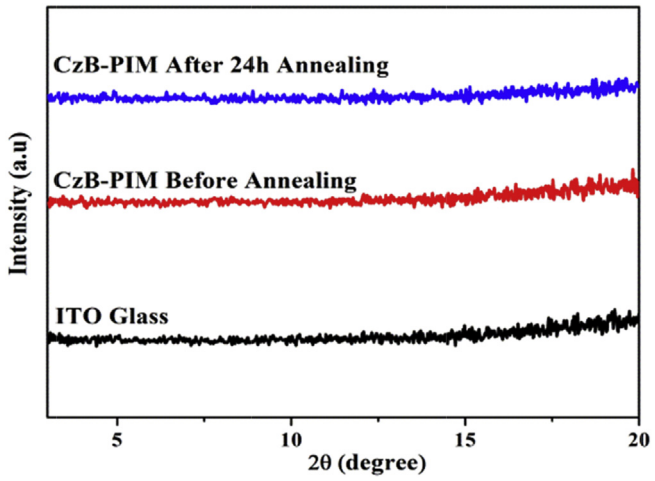

Fig. 3. X-ray diffraction spectra of the ITO substrate and CzB-PIM thin film on ITO substrates.

A slight bathochromic-shift (~6 nm) can be observed in film PL spectrum compare with in THF solution, while the change of FWHM is unobvious. However, the 2-(4′-(9*H*-carbazol-9-yl)-[1,1′-biphenyl]-4-yl)-1-phenyl-1*H*-phenanthro[9,10-*d*] imidazole (M5) which has similar structure with CzB-PIM showed a great change in absorption and emission spectra and reported in literature [20]. This indicates that compared with phenanthro[9,10-*d*]imidazole moiety the 1,4,5-triphenyl-1*H*-imidazole moiety can increase the molecular twists to reduce planarity. The intermolecular stacking in solid state is suppressed by this kind of noncoplanar structure in CzB-PIM which also confirmed by single crystal diffusion discussed above [12,30]. In addition, the PL spectrum of CzB-PIM film showed maximum peak at 415 nm, that of M5 film was reported to be 430 nm, which suggests that breaking one C–C bond of phenanthrene can enlarge the E_g to achieve deep blue emitting.

The solution fluorescence quantum yields (Φ_f) of CzB-PIM measured in THF using quinine sulfate (0.01 M dilute H_2SO_4, Φ_f = 0.54) as a standard is 0.87. The optical band gap (E_g) determined from the onset of the UV–Vis absorption is 3.31 eV, The large E_g ensured blue emission, and low LUMO level benefited for accepting electron from anode. HOMO energy level was measured by photoelectron yield spectroscopy to be −5.76 eV, LUMO energy level was further estimated to be −2.45 eV by summing the corresponding HOMO level and E_g. To gain insight into the electronic structures of CzB-PIM, the

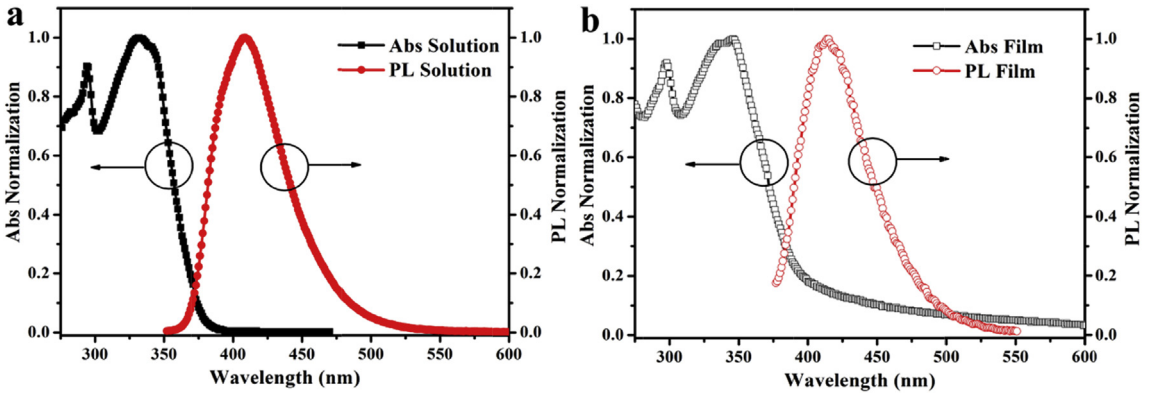

Fig. 4. Solution (a, 10^{-5} M) and solid film (b) Normalized absorption spectra (square) and fluorescence spectra (circle) of Czb-PIM.

density functional theory (DFT) calculation was performed at the B3LYP/6-31G (d) level. The corresponding the frontier molecular orbitals of CzB-PIM are shown in Fig. S1. The HOMO localizes on the almost whole molecular, except benzene connecting with N3 atom. While the LUMO mainly localizes on the biphenyl and imidazole. Moreover, a suitable overlap between the HOMO and LUMO can be observed which results in the high fluorescence efficiency, demonstrated by the high Φ_f [34].

3.4. Bipolar charge injection/transport properties

The bipolar charge injection/transport properties of CzB-PIM were identified by single-carrier devices. Here, *N,N′*-bis-(1-naphthalenyl)-*N,N′*-bis-phenyl-(1,1′-biphenyl)-4,4′- diamine (NPB) and 1,3,5-tris(1-phenyl-1*H*-benzimidazol-2-yl)benzene (TPBi) were used as hole and electron transport material respectively. The device configurations are shown following: ITO/NPB (15 nm)/CzB-PIM (30 nm)/NPB (15 nm)/Al (200 nm) and ITO/TPBi (15 nm)/CzB-PIM (30 nm)/TPBi (15 nm)/LiF (1 nm)/Al (200 nm). NPB and TPBi layers are used to prevent electron and hole injecting from cathode and anode, respectively [12,29]. The current density versus voltage (*J–V*) curves of two single-carrier devices are showed in Fig. 5a.

Obviously, both single-hole and single-electron devices exhibit good diode characteristics, which demonstrates the good bipolar transport property of CzB-PIM. The lower current density in the hole-only curve than the electron-only curve at the same voltage can be obvious in the voltage range of 4–14 V. This indicated better electron transporting characteristic than hole. Besides, the barrier of carriers injection from NPB layer to CzB-PIM layer (0.36 eV) is larger than TPBi layer to CzB-PIM layer (0.25 eV). This resulted the current onset in electron only device (~4 V) is much smaller than current onset in hole only device (~11 V) [29,35].

3.5. Electroluminescence (EL) performance

According to the above studies, the non-doped fluorescent OLED was fabricated with a structure of ITO/NPB (30 nm)/TCTA (10 nm)/CzB-PIM (20 nm)/TPBi (35 nm)/LiF (1 nm)/Al (200 nm). In this device, ITO and LiF/Al was used as the anode and cathode respectively, NPB as the hole transporting layer (HTL), TCTA (4,4′,4″-tris(*N*-carbazolyl)triphenylamine) as the electron blocking layer, TPBi as the electron-transporting layer (ETL) and the hole blocking layer, the CzB-PIM as the emitting layer (EML). The diagram of energy levels and molecular structures are illustrated in Fig. 6.

The current density-voltage-luminance (*J–V–L*) curves and EL spectra of device operated at voltage of 5–9 V are shown in Fig. 7. As shown in Fig. 7a, the turn on voltage (V_{on}) is 4.75 V which defined as the operation voltage at luminance of 1 cd/m^2. Compared with reported deep.

blue OLEDs (in Table 2), the slight higher V_{on} resulted from the injection barrier form ITO side as well as the relative week hole transport property. The V_{on} is reduced to 4.15 V after inserting MoO_3 layer between ITO and NPB as hole injection layer. The luminance, CE and LE have also been improved (Seeing ESI Fig. S6). Additionally, the electroluminance spectra are same with PL spectra which indicates that the emission of EL and PL spectra of CzB-PIM film generate from the decay of singlet excitons and does not exit excimers or exciplex during the EL progress [7,9].

The non-doped device exhibited deep blue EL spectra, with emission peak at 420 nm and CIEy coordinates ≤0.064, with operation voltage ≤9 V, which is very closing to the standard CIEy of EBU (Fig 8a). Noticeably, with the increase of applied driving voltage from 5 to 9 V, the change of EL spectra are negligible (Fig. 7b). As shown in Fig. 8b, only values of CIEy slightly increased with increasing operation voltage. Fig. 9 shows current efficiency (CE) versus luminance versus power efficiency (PE) curves of the device. The maximum CE and PE of CzB-PIM based OLED without optimazition of device structure are 2.30 cd/A and 1.52 lm/W, respectively. The electron mobility (μ_e) of TPBi and the hole mobility (μ_h) of NPB are reported to be 0.25–1.70 × 10^{-5}, 6.10 × 10^{-5} cm^2/(V s), respectively [36]. As the CzB-PIM shows an obvious electron transport property, the lower efficiency at higher luminance may be due to the disequilibrium of charge injection and transport in device [35], which can be

Table 1
Key physical properties of CzB-PIM.

Compound	T_d, T_m, T_g (°C)	λ_{abs}^{sol} (nm)	λ_{abs}^{film} (nm)	λ_{em}^{sol} (nm)	λ_{em}^{film} (nm)	Φ_f[a]	E_g[b] (eV)	HOMO[c] (eV)	LUMO[d] (eV)
CzB-PIM	413,293,134	294,335	298,336	409	415	0.87	3.31	−5.76	−2.45

[a] Measured in THF with quinine sulfate as a standard.
[b] The optical band gap (E_g) determined from the onset of the absorption.
[c] Determined from PYS measurement.
[d] LUMO = HOMO + E_g.

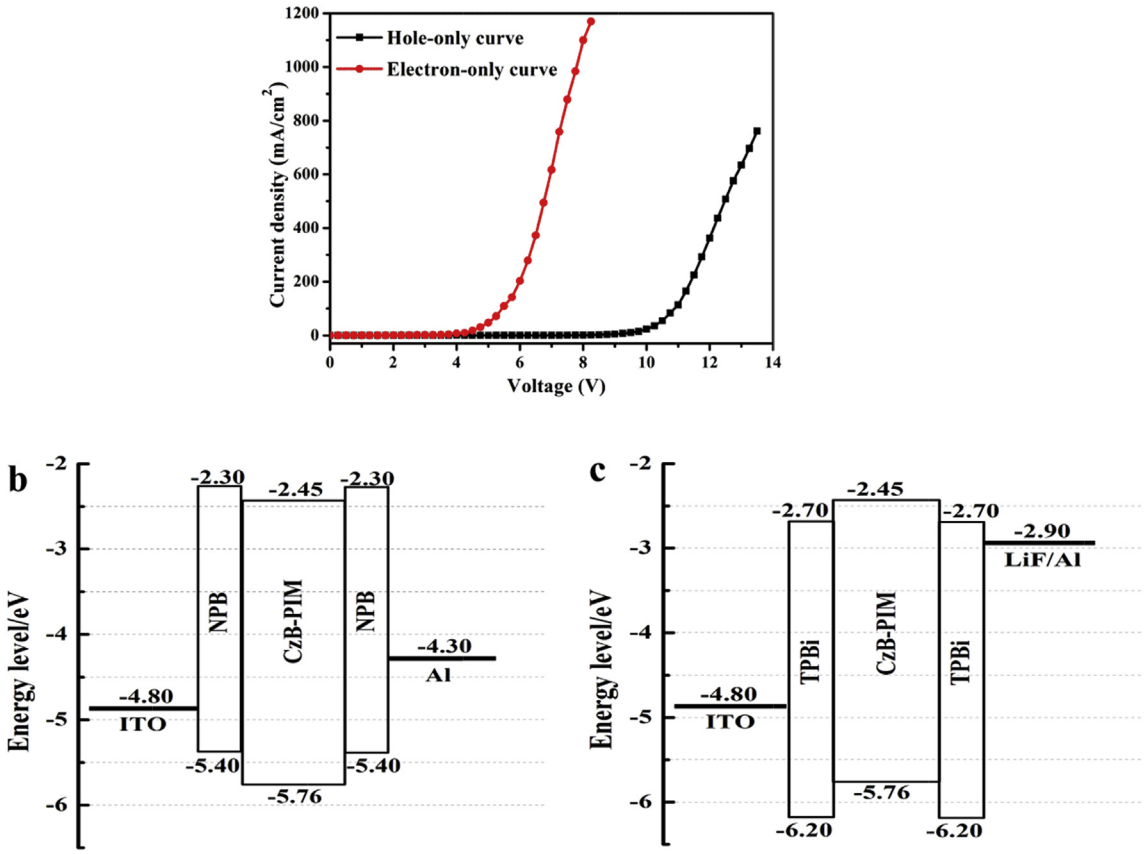

Fig. 5. *J–V* curves (a) and energy level diagram of the hole-only (b) and electron-only (c) devices for CzB-PIM.

simply improved with changing thickness of hole transport layer and electron transport layer. However, the high quantum efficiency still ensure the high CE at low luminance. The CE of device reported in this work is still in the highest level of reported blue OLEDs with CIEy $\leq$0.064 (in Table 2).

4. Conclusion

A new bipolar emitting molecular, CzB-PIM, incorporating carbazole as electron-donor and imidazole as electron-acceptor and biphenyl as π bridge, was successfully synthesized and characterized by NMR, HRMS, and X-ray single crystal diffraction. Broken of C–C band in phenanthro[9,10-*d*]imidazole moiety to form 1,4,5-triphenyl-1*H*-imidazole moiety increased the twist of molecule and enlarged Eg, resulted a deep blue emission. Meanwhile, the CzB-PIM maintained good bipolar carrier transporting property which was identified by single-carrier device. The non-doped OLED device based on CzB-PIM shows a good performance with maximum EL peak at 420 nm, FWHM of 54 nm, CE of 2.30 cd/A and CIE coordinate (0.166, 0.064), approaching EBU deep blue standard, which is better than most reported deep blue OLEDs with CIEy $\leq$ 0.064.

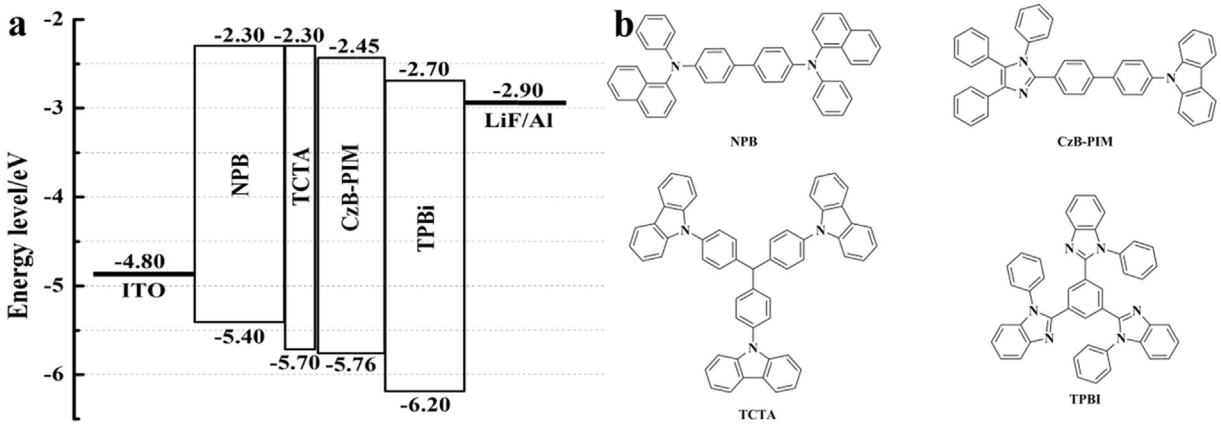

Fig. 6. Energy level diagrams (a) and chemical structures (b) of the materials used in devices.

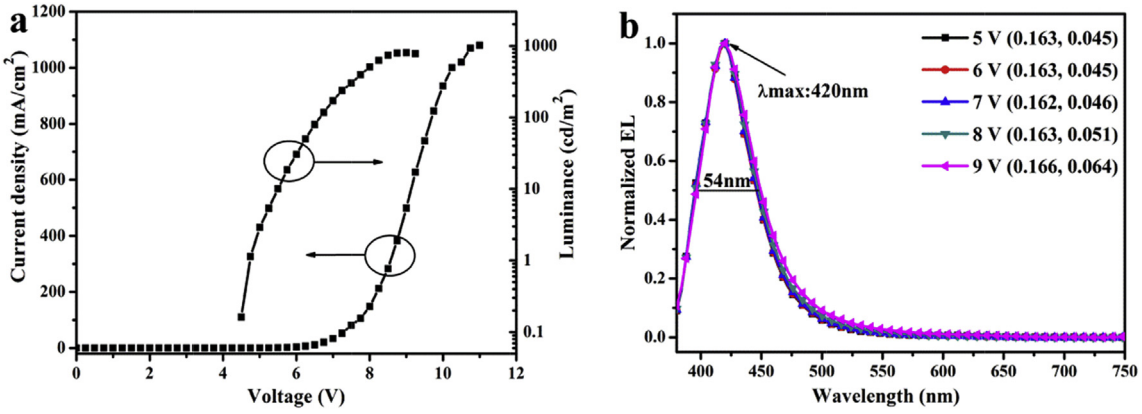

Fig. 7. *J–V–L* curves (a) and EL spectra (b) in different voltages for CzB-PIM.

Table 2
Key performance parameters of reported deep blue OLEDs with CIEy ≤0.064.

Compounds	V_{on} (V)	λmax[a] (nm)	CE[b] (cd/A)	PE[c] (lm/W)	EQE[d] (%)	CIE (x, y)	Ref
CzB-PIM	**4.75**	**420**	**2.30**	**1.52**	–	**(0.166, 0.064)**	**This work**[e]
BPA-BPI	3.1	428	0.65	0.68	1.37	(0.15, 0.05)	[11][e]
PATPA	2.0	424	0.34	0.24	0.72	(0.15, 0.06)	[11][e]
TTP-TPI	3.1	424	2.10	1.88	5.02	(0.16, 0.05)	[12][e]
CzS1	3.5	426	1.89	1.58	4.21	(0.157, 0.055)	[14][e]
CzS2	2.8	417	0.82	0.84	2.7	(0.157, 0.044)	[14][e]
TPA-PIM	<3	420	1.14	0.79	3	(0.161, 0.045)	[27][e]
PhPC	–	436	1.82	1.05	–	(0.15, 0.05)	[33][e]
3a	–	416	0.5	0.2	–	(0.16, 0.05)	[37][f]
TDAF1	2.5	–	1.53	–	5.3	(0.15, 0.041)	[38][e]
TDAF2	2.5	–	1.1	–	4.1	(0.16, 0.044)	[38][e]
CPhBzIm	2.5	426	1.6	1.07	3	(0.16, 0.05)	[39][e]
M1	–	420	0.65	0.48	1.94	(0.16, 0.050)	[40][e]
M2	–	428	1.53	0.86	3.02	(0.16, 0.056)	[40][e]
TCPC-4	–	425	0.9	–	2.47	(0.16, 0.05)	[41][e]
TCPC-6	–	425	1.35	–	3.72	(0.16, 0.05)	[41][e]
TPA-(3)-F	5.8	428	0.39	–	–	(0.16, 0.06)	[42][e]
TPAXAN	–	428	–	–	4.62	(0.155, 0.049)	[43][e]
Cz-2pbb	2.5–3	410	–	–	4.1	(0.16, 0.05)	[44][f]
Purine 1	2.9	432	–	–	3.1	(0.15, 0.06)	[45][f]

"**This work**" is defined as the device reported in this article.
[a] Maximum electroluminescence wavelength.
[b] Maximum current efficiency.
[c] Maximum power efficiency.
[d] Maximum external quantum efficiency.
[e] Non-doped.
[f] Doped devices.

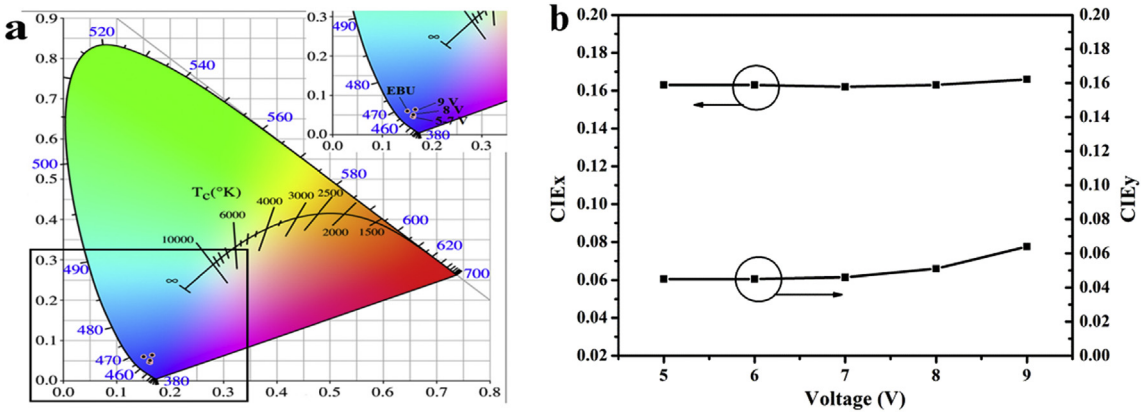

Fig. 8. CIE diagram for EL emission (a) and CIEx and CIEy (b) at different voltage.

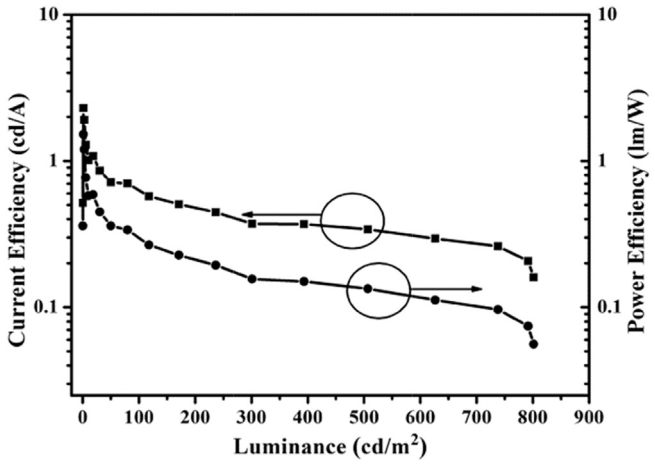

Fig. 9. Current efficiency-luminance-Power efficiency curves for the nondoped device.

Acknowledgments

This research was financially supported by the National High Technology Research and Development Program of China (No. 2015AA033402) and the Science and Technology Planning Project of Tianjin Province, China (No. 14TXGCCX00017). The calculation in this work was supported by high performance computing center of Tianjin University, China.

Appendix A. Supplementary data

Supplementary data related to this article can be found at http://dx.doi.org/10.1016/j.dyepig.2016.02.006.

References

[1] Zhang Z, Jiang W, Ban X, Yang M, Ye S, Huang B, et al. Solution-processed efficient deep-blue fluorescent organic light-emitting diodes based on novel 9,10-diphenyl-anthracene derivatives. RSC Adv 2015;5:29708–17.
[2] Tang CW, VanSlyke SA. Organic electroluminescent diodes. Appl Phys Lett 1987;51:913–5.
[3] Lyu Y-Y, Kwak J, Kwon O, Lee S-H, Kim D, Lee C, et al. Silicon-cored anthracene derivatives as host materials for highly efficient blue organic light-emitting devices. Adv Mater 2008;20:2720–9.
[4] Seo JH, Lee KH, Seo BM, Koo JR, Moon SJ, Park JK, et al. High-efficiency deep-blue organic light- emitting diodes using dual-emitting layer. Org Electron 2010;11:1605–12.
[5] Zhu M, Ye T, Li C-G, Cao X, Zhong C, Ma D, et al. Efficient solution-processed nondoped deep-blue organic light-emitting diodes based on fluorene-bridged anthracene derivatives appended with charge transport moieties. J Phys Chem C 2011;115:17965–72.
[6] Lee Y-H, Wu T-C, Liaw C-W, Wen T-C, Feng S-W, Lee J-J, et al. Non-doped active layer, benzo[k] fluoranthene-based linear acenes, for deep blue- to green-emissive organic light-emitting diodes. Org Electron 2013;14:1064–72.
[7] Xu X, Ye S, He B, Chen B, Xiang J, Zhou J, et al. Dimesitylboryl-functionalized fluorene derivatives: promising luminophors with good electron-transporting ability for deep blue organic light-emitting diodes. Dyes Pigments 2014;101:136–41.
[8] Liang H, Wang X, Zhang X, Ge Z, Ouyang X, Wang S. Efficient tuning of electroluminescence from sky-blue to deep-blue by changing the constitution of spirobenzofluorene derivatives. Dyes Pigments 2014;108:57–63.
[9] Liu C, Fu Q, Zou Y, Yang C, Ma D, Qin J. Low turn-on voltage, high-power-efficiency, solution- processed deep-blue organic light-emitting diodes based on starburst oligofluorenes with diphenylamine end-capper to enhance the HOMO level. Chem Mater 2014;26:3074–83.
[10] Zheng C-J, Zhao W-M, Wang Z-Q, Huang D, Ye J, Ou X-M, et al. Highly efficient non-doped deep- blue organic light-emitting diodes based on anthracene derivatives. J Mater Chem 2010;20:1560–6.
[11] Zhang Y, Lai S-L, Tong Q-X, Lo M-F, Ng T-W, Chan M-Y, et al. High efficiency nondoped deep-blue organic light emitting devices based on imidazole-π-triphenylamine derivatives. Chem Mater 2012;24:61–70.
[12] Yuan Y, Chen J-X, Lu F, Tong Q-X, Yang Q-D, Mo H-W, et al. Bipolar phenanthroimidazole derivatives containing bulky polyaromatic hydrocarbons for nondoped blue electroluminescence devices with high efficiency and low efficiency roll-off. Chem Mater 2013;25:4957–65.
[13] Benor A, Takizawa S-y, Pérez-Bolivar C, Anzenbacher P. Energy barrier, charge carrier balance, and performance improvement in organic light-emitting diodes. Appl Phys Lett 2010;96:243310.
[14] Ye J, Chen Z, Fung M-K, Zheng C, Ou X, Zhang X, et al. Carbazole/sulfone hybrid D-π-A-structured bipolar fluorophores for high-efficiency blue-violet electroluminescence. Chem Mater 2013;25:2630–7.
[15] Lin S-L, Chan L-H, Lee R-H, Yen M-Y, Kuo W-J, Chen C-T, et al. Highly efficient carbazole-π- dimesitylborane bipolar fluorophores for nondoped blue organic light-emitting diodes. Adv Mater 2008;20:3947–52.
[16] Gong S, Chen Y, Luo J, Yang C, Zhong C, Qin J, et al. Bipolar tetraarylsilanes as universal hosts for blue, green, orange, and white electrophosphorescence with high efficiency and low efficiency roll-off. Adv Funct Mater 2011;21:1168–78.
[17] Lu T, You J, Zhao D, Wang H, Miao Y, Liu X, et al. Synthesis of novel s-triazine/carbazole based bipolar molecules and their application in phosphorescent OLEDs. J Mater Sci Mater Electron 2015;26:6563–71.
[18] Huang J, Su J-H, Li X, Lam M-K, Fung K-M, Fan H-H, et al. Bipolar anthracene derivatives containing hole- and electron-transporting moieties for highly efficient blue electroluminescence devices. J Mater Chem 2011;21:2957–64.
[19] Li W, Liu D, Shen F, Ma D, Wang Z, Feng T, et al. A twisting donor-acceptor molecule with an intercrossed excited state for highly efficient, deep-blue electroluminescence. Adv Funct Mater 2012;22:2797–803.
[20] Gao Z, Wang Z, Shan T, Liu Y, Shen F, Pan Y, et al. High-efficiency deep blue fluorescent emitters based on phenanthro[9,10-d]imidazole substituted carbazole and their applications in organic light emitting diodes. Org Electron 2014;15:2667–76.
[21] Hu J-Y, Pu Y-J, Satoh F, Kawata S, Katagiri H, Sasabe H, et al. Bisanthracene-based donor-acceptor -type light-emitting dopants: highly efficient deep-blue emission in organic light-emitting devices. Adv Funct Mater 2014;24(14):2064–71.
[22] Kotchapradist P, Prachumrak N, Tarsang R, Jungsuttiwong S, Keawin T, Sudyoadsuk T, et al. Pyrene- functionalized carbazole derivatives as nondoped blue emitters for highly efficient blue organic light-emitting diodes. J Mater Chem C 2013;1:4916–24.
[23] Liu XC, You J, Xiao Y, Wang SR, Wang WZ, Peng JB, et al. Film-forming hole transporting materials for high brightness flexible organic light-emitting diodes. Dyes Pigments 2016;125:36–43.
[24] Farrugia LJ. WinGX suite for small-molecule single-crystal crystallography. J Appl Crystallogr 1999;32:837–8.
[25] Frisch MJ, Trucks GW, Schlegel HB, Scuseria GE, Robb MA, Cheeseman JR, et al. Gaussian 03, revision D.02. Wallingford CT: Gaussian, Inc.; 2004.
[26] You J, Li G, Wang Z. Starburst dendrimers consisting of triphenylamine core and 9-phenyl carbazole-based dendrons: synthesis and properties. Org Biomol Chem 2012;10:9481–90.
[27] Li W, Yao L, Liu H, Wang Z, Zhang S, Xiao R, et al. Highly efficient deep-blue OLED with an extraordinarily narrow FHWM of 35 nm and a y coordinate <0.05 based on a fully twisting donor-acceptor molecule. J Mater Chem C 2014;2:4733–6.
[28] Hua W, Liu Z, Duan L, Dong G, Qiu Y, Zhang B, et al. Deep-blue electroluminescence from nondoped and doped organic light-emitting diodes (OLEDs) based on a new monoaza[6]helicene. RSC Adv 2015;5:75–84.
[29] Liu D, Du M, Chen D, Ye K, Zhang Z, Liu Y, et al. A novel tetraphenylsilane-phenanthroimidazole hybrid host material for highly efficient blue fluorescent, green and red phosphorescent OLEDs. J Mater Chem C 2015;3:4394–401.
[30] Nagarajan N, Prakash A, Velmurugan G, Shakti N, Katiyar M, Venuvanalingam P, et al. Synthesis, characterisation and electroluminescence behaviour of π-conjugated imidazole–isoquinoline derivatives. Dyes Pigments 2014;102:180–8.
[31] Chen SF, Tian Y, Peng J, Zhang H, Feng XJ, Zhang H, et al. Synthesis and characterization of arylamino end-capped silafluorenes for blue to deep-blue organic light-emitting diodes (OLEDs). J Mater Chem C 2015;3:6822–30.
[32] Zhao L, Wang S, Shao S, Ding J, Wang L, Jing X, et al. Stable and efficient deep-blue terfluorenes functionalized with carbazole dendrons for solution-processed organic light-emitting diodes. J Mater Chem C 2015;3:8895–903.
[33] Huang Y, Du X, Tao S, Yang X, Zheng C-J, Zhang X, et al. High efficiency non-doped deep-blue and fluorescent/phosphorescent white organic light-emitting diodes based on an anthracene derivative. Synth Met 2015;203:49–53.
[34] Chen Z, Liu X-K, Zheng C-J, Ye J, Li X-Y, Li F, et al. A high-efficiency hybrid white organic light- emitting diode enabled by a new blue fluorophor. J Mater Chem C 2015;3:4283–9.
[35] Wang K, Wang S, Wei J, Miao Y, Liu Y, Wang Y. Novel diarylborane–phenanthroimidazole hybrid bipolar host materials for high-performance red, yellow and green electrophosphorescent devices. Org Electron 2014;15:3211–20.
[36] Shirota Y, Kageyama H. Charge carrier transporting molecular materials and their applications in devices. Chem Rev 2007;107:953–1010.

[37] Karthik D, Justin Thomas KR, Jou J-H, Kumar S, Chen Y-L, Jou Y-C. Deep-blue emitting pyrene- benzimidazole conjugates for solution processed organic light-emitting diodes. RSC Adv 2015;5:8727–38.
[38] Wu CC, Lin YT, Wong KT, Chen RT, Chien YY. Efficient organic blue-light-emitting devices with double confinement on terfluorenes with ambipolar carrier transport properties. Adv Mater 2004;16:61–5.
[39] Hung W-Y, Chi L-C, Chen W-J, Chen Y-M, Chou S-H, Wong K-T. A new benzimidazole/carbazole hybrid bipolar material for highly efficient deep-blue electrofluorescence, yellow-green electrophosphorescence, and two-color-based white OLEDs. J Mater Chem 2010;20:10113–9.
[40] Gao Z, Liu Y, Wang Z, Shen F, Liu H, Sun G, et al. High-efficiency violet-light-emitting materials based on phenanthro[9,10-d]imidazole. Chem Eur J 2013;19:2602–5.
[41] Tang S, Liu MR, Lu P, Xia H, Li M, Xie ZQ, et al. A molecular glass for deep-blue organic light- emitting diodes comprising a 9,9′-Spirobifluorene core and peripheral carbazole groups. Adv Funct Mater 2007;17:2869–77.
[42] Li Z, Wu Z, Fu W, Liu P, Jiao B, Wang D, et al. Versatile fluorinated derivatives of triphenylamine as hole-transporters and blue-violet emitters in organic light-emitting devices. J Phys Chem C 2012;116:20504–12.
[43] Kim R, Lee S, Kim K-H, Lee Y-J, Kwon S-K, Kim J-J, et al. Extremely deep blue and highly efficient non-doped organic light emitting diodes using an asymmetric anthracene derivative with a xylene unit. Chem Commun 2013;49:4664–6.
[44] Yang X, Zheng S, Bottger R, Chae HS, Tanaka T, Li S, et al. Efficient fluorescent deep-blue and hybrid White emitting devices based on carbazole/benzimidazole compound. J Phys Chem C 2011;115:14347–52.
[45] Yang Y, Cohn P, Dyer AL, Eom S-H, Reynolds JR, Castellano RK, et al. Blue-violet electroluminescence from a highly fluorescent purine. Chem Mater 2010;22:3580–2.